NANO LETTERS

2007
Vol. 7, No. 2
426−432

Thermomechanics of Nanocrystalline Nickel under High Pressure–Temperature Conditions

Yusheng Zhao,*,† Jianzhong Zhang,† Bjørn Clausen,† T. D. Shen,‡ George T. Gray III,‡ and Liping Wang§

LANSCE Division, Los Alamos National Laboratory, Los Alamos, New Mexico 87545, MST Division, Los Alamos National Laboratory, Los Alamos, New Mexico 87545, and Mineral Physics Institute and COMPRES, University at Stony Brook, New York 11794

Received November 16, 2006; Revised Manuscript Received December 7, 2006

ABSTRACT

We present a comparative study of thermomechanical properties of nano-polycrystalline nickel (nano-Ni) and micrometer-polycrystalline nickel (micron-Ni) by in situ high pressure–temperature (*P*–*T*) diffraction experiments. The yield strength of 2.35 GPa for the nano-Ni measured under high-pressure triaxial compression is more than three times that of the micron-Ni value. Contrary to tensile experiments of uniaxial loading, we observe significant work-hardening for the nano-Ni in high-pressure plastic deformation stage, whereas the micron-Ni experiences minor high-pressure work-softening and considerable energy dissipation into heat. The significantly reduced energy dissipation for the nano-Ni during the loading–unloading cycle indicates that the nanostructured materials can endure much greater mechanical fatigue in cyclic loadings. The nano-Ni exhibits steady grain growth during bulk plastic deformation at high-pressure loading, and drastic stress reduction and grain growth occur during the high *P*–*T* cycle. Our experiments utilized novel approaches to comparatively study micro- and nanostructured materials revealing recoverability of elastic/plastic deformations, strain corrections by diffraction elasticity ratio, and identifying dominances of stress relaxation, grain growth, and intrinsic residual stresses. The results should be of considerable interest to the fields of materials science, condensed matter, and computational physics.

Nanocrystalline materials hold the promise of revolutionizing traditional materials design in many applications via atomic-level structural control of tailored properties of technological interest. As opposed to the micrometer scale, the nanoscale is not just another step toward miniaturization. Nanoscale is a qualitatively new scale as continuum mechanics theory reaches its atomistic limit in describing material behavior. As a result, the size-dependent atomic structures often lead to distinct, usually enhanced, properties of nano-polycrystals relative to conventional bulk polycrystalline materials.[1−6] The yield strength and hardness of many polycrystalline metals typically increases when the grain size decreases to the nanometer scale, as predicted by the well-known Hall−Petch relation.[7,8] However, yield strength is not an intrinsic material property and can vary depending on the internal structure and chemistry of the material as well as the loading conditions. This is particularly true in nanoscale materials, as differences in specific chemical makeup and/or defect concentration/distribution can greatly alter the point at which the material yields.[9] In addition, the nucleation, propagation, and storage of dislocations for plastically deforming nanocrystalline materials under triaxial loading, and their variations with pressure and temperature, remain poorly characterized.

Conventional tensile testing to derive materials' mechanical properties requires centimeter-scale specimens and is also subject to the influence of material porosity and defect starting structure due to differences in processing history. Presently, most nanostructured materials are in the form of powders, making it difficult to study deformation mechanisms and constitutive properties following traditional mechanical testing approaches. To fully realize the promise and potential of novel nanomaterials as well as to understand their mechanical properties under different loading conditions, it is essential to apply new approaches to characterize relationships between microstructure and nanostructure properties. Here, we present compression studies on deformation of nanocrystalline and bulk nickel samples using in situ synchrotron X-rays at high pressure−temperature (*P*−*T*) conditions.

The high *P*−*T* diffraction experiments were conducted using a DIA-type, cubic anvil apparatus[10] at beam line X17B2 at the National Synchrotron Light Source (NSLS), Brookhaven National Laboratory. The nano-Ni powders, with

* Corresponding author: e-mail, yzhao@lanl.gov; phone (505) 667-3886.
† LANSCE Division, Los Alamos National Laboratory.
‡ MST Division, Los Alamos National Laboratory.
§ Mineral Physics Institute and COMPRES, University at Stony Brook.

10.1021/nl062685s CCC: $37.00
Published on Web 12/21/2006

a median particle size of 8−10 nm, was prepared by a mechanical milling technique.[3] The microcrystalline nickel powders (micron-Ni) used were 99.8% pure and had a grain size distribution of 3−7 μm. The nano-Ni and micron-Ni samples were symmetrically loaded in a cylindrical boron−nitride (BN) capsule and separated by a layer of NaCl, which also served as a pressure standard. We used the Decker equation-of-state[11] to determine pressure and a tungsten−rhenium thermocouple to measure the temperature of the samples. The nano/micron-Ni powders were compressed under a quasi-hydrostatic pressure, which introduces a heterogeneous triaxial strain field due to overall compression and the point contacts between the powder particles. With the use of diffraction techniques, the strain within a sample was determined mainly in two ways:[12,13] (1) by changes in diffraction peak *position*, and (2) by changes in diffraction peak *width*. The first gives a direct measure of strain by calculating the relative shift in peak position, $\epsilon = (d - \bar{d})/d$. In the second, the peak-width variations are the function of *d*-spacing; for example, isotropic strain is proportional to the *d*-spacing, and the grain size (scattering domain size) is proportional to square of the *d*-spacing. We utilized the peak-width approach to determine the sample deformation as described in the subsequent paragraphs.

Contrary to grain-crushing[6] in hard and brittle materials, the ductile nickel metal will respond to the triaxial loading by local yielding to relieve the high-stress concentrations at grain to grain contact points, through plastic deformation. Initially, this yielding will generate a heterogeneous dislocation density within the grains as more and more of the grain becomes plastic. After considerable deformation, the bulk of the crystals' grains will be plastically deforming, and the dislocation density within a grain will become nearly uniform. It is important to note that due to the triaxial stress state during the experiments, the derived yield strengths may not be directly comparable to traditionally determined yield strength under a well-defined uniaxial stress state. However, because the two crystalline samples are studied in one single experiment and experience identical pressures and temperatures, the comparative study between the nano/micron samples can accordingly provide insight into the intrinsic property differences in their thermomechanics under high $P-T$ conditions.

The observed diffraction patterns plotted in Figure 1 are selected to present peak profile changes of nano-Ni and micron-Ni at various $P-T$ conditions. The profile of the observed diffraction peaks is a convolution of integrated effects of instrument response, grain sizes, and microstrains due to stress heterogeneity, lattice deformation, and dislocation density at high $P-T$.[13,14] In a length scale of lattice *d*-spacing, measured in angstroms (Å), the observed full width at half maximum (fwhm) can be denoted as Δd_{obs}. It reflects the *d*-spacing span around the mean $\bar{d}_{hkl}$ of a particular *hkl*, independent of detecting modes of energy dispersive (keV), angular dispersive (2θ), or time-of-flight (μs). Using a Gaussian formulation to represent the peak width, the deconvoluted width (fwhm) of the diffraction peak is $\Delta d^2_{obs} = \Delta d^2_{ins} + \Delta d^2_{size} + \Delta d^2_{\epsilon}$ (P,T). In the present high

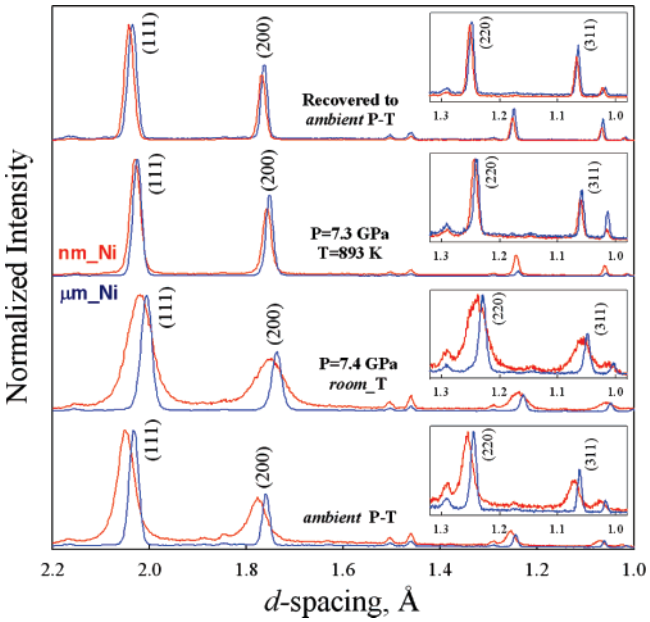

Figure 1. The diffraction patterns for nano-Ni (red) and miron-Ni (blue) at different $P-T$ conditions are labeled with their *hkl* index. The inserted boxes are the magnifications of the high-angle diffractions. The initial significant peak-broadening of nano-Ni is augmented as severe contact stresses are applied on the crystal grains at high pressures. The diffraction peaks sharpen at high temperatures indicating stress relaxation as well as grain growth. The peak intensities of the *hkl* diffractions are normalized for width comparison. The patterns for the recovered nano-Ni sample have the same diffraction peak widths as the micron-Ni at the ambient conditions. The fact that the peaks of the micron-Ni at high $P-T$ are even sharper than its ambient width indicates the total release of the residual stress and reveals intrinsic instrument diffraction. The lattices of the nano-Ni apparently shift toward larger *d*-spacing in comparison with micron-Ni. This shift is mainly due to surface strain effects introduced in the severe process of grain size reduction; there are also minor impurity effects in the nano-Ni sample.[3] Some minor peaks in the patterns are lead (Pb) resonance peaks, which do not change with $P-T$ conditions.

$P-T$ diffraction study, we focus on "nonuniform" strain effect of Δd_{ϵ} (P,T) caused by stress heterogeneity and anisotropy as well as dislocation density.[15] In our calculations we subtract the instrument resolution, but otherwise we do not try to deconvolute the various contributions to the peak width changes. Hence, we determined the strain by the ratio of the peak-width change to the peak position in terms of *d*-spacing

$$\epsilon = \Delta d_{\epsilon}/d = \sqrt{\Delta d^2_{obs} - \Delta d^2_{ins}}/d(P,T) \qquad (1)$$

To illustrate the differences between the nano-Ni and the micron-Ni in the early stages of loading, we measured the strains from two separate runs at maximum pressures, 1.4 and 6.0 GPa, corresponding to before and after plastic yields of the samples. As the absolute values of the strains for individual *hkl* planes in the crystal lattice vary according to different elastic compliances, the absolute value of the apparent strain at the maximum pressure is about 3−4 times higher for the nano-Ni than for the micron-Ni. To make the comparisons easier, we normalized the observed strain

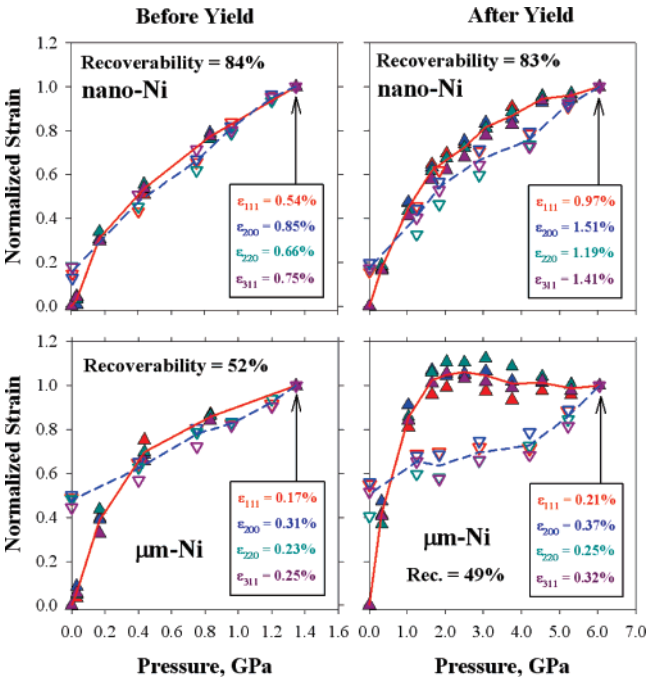

Figure 2. The normalized apparent strain, $\bar{\epsilon}_{hkl}^{\text{apparent}} = (\Delta d/d)_{hkl}/(\Delta d/d)_{hkl}^{\text{max.}P}$, plotted as a function of pressure, for the nano-Ni (top) and micron-Ni (bottom). The left panel is for the low-pressure experiment up to 1.4 GPa and the right panel for the experiments at higher maximum pressure. The color codes for each *hkl* are as follows: red (111), blue (200), cyan (220), and purple (311). The solid up-triangle symbols are for pressure loading and the open down-triangles are for unloading. The solid red line and the dashed blue line represent the averaged strains $\bar{\epsilon}$ for the loading and unloading stages, respectively. The individual lattice strains of ϵ_{hkl} at the highest pressure (max.*P*) are listed in the inserted boxes. The recoverability: Rec. $= [\bar{\epsilon}(\text{max.}P) - \bar{\epsilon}(\text{end})]/\{\epsilon(\text{max.}P)$

relative to the maximum strain at the highest pressure, $\epsilon_{hkl}^{\text{norm}} = (\Delta d/d)_{hkl}/(\Delta d/d)_{hkl}^{\text{max.}P}$. The normalized strains are shown in Figure 2 for nano-Ni (top) and micron-Ni (bottom) for the two experiments, 1.4 GPa (left) and 6.0 GPa (right). It is evident that the lattice planes have different compressibility upon loading (*pressurizing*), as seen by the spread between the symbols at each pressure level. It is also important to note that although overall deformation during the experiments is quasi-hydrostatic and homogeneous, the individual powder particles experience a very heterogeneous deformation due to point contacts between individual particles. There are two obvious yield (kink) points for micron-Ni at $P = 0.4$ GPa and $P = 1.6$ GPa, and the corresponding normalized strains at 0.7 and 1.0, respectively. We consider that the first yield represents "micro/local" grain-to-grain contacts that deform plastically due to high-stress concentration and the second yield represents "macro/bulk" plastic deformation of the entire sample. The two-stage yielding phenomenon is not as obvious in the nano-Ni, as it exhibits pronounced nonlinear ductility; the "local" yield is expected at even lower pressures.

The comparative recoverability study of plastic deformation shows that the nano-Ni recovers a much larger fraction of the incurred strain upon unloading, 83−84% depending on maximum pressure, whereas the micron-Ni only recovers 49−52%. The unrecoverable strain can be caused by intergranular and/or intragranular mechanisms of plasticity. Previous studies[15] have shown that nano-Ni shows full recovery of dislocation density when loaded in uniaxial tension. Interestingly, we observed that the recoverability for the nickel samples remains at about the same level for the unloading before and/or after the bulk plastic yielding. This, and the combination of almost full recovery for nano-Ni and less recovery for the micron-Ni in our triaxial-stress experiments, suggest that the unrecoverable part of the plastic strain in the nano-Ni is mainly due to intergranular strains (for example, grain riding/sliding and elastic/plastic anisotropy), whereas in the micron-Ni it is dominated by intragranular strains (for example, dislocation density and heterogeneous stress distribution).

The work-hardening to much higher strains is observed for the nano-Ni, and the work-softening to surrender the max-supported strain is observed for the micron-Ni (Figure 2). It is in contrary to previously observed minor work-hardening found in nanocrystalline metals and significant work-hardening found in microcrystalline metals—as measured under uniaxial tension. There is a significant loading−unloading hysteresis loop for the after-yield micron-Ni sample, despite the similar recoverability as the before-yield sample. Figure 2 suggests that the high-P works upon the micron-Ni are dissipated as heat and the sample is in a ductile flow state without further development of dislocation density. The dissipation loop is much smaller for the nano-Ni sample (*in a 1:3.15 ratio compared with micron-Ni*) indicating reduced energy loss in its plasticity deformation stage. The reduced level of energy dissipation for the nano-Ni during the loading−unloading cycle indicates that the nanostructured materials may be able to more readily endure greater mechanical fatigue in cyclic load path changes.

As we are looking at two different grain sizes, we must take into account the peak broadening from the crystal size. The Scherrer formula[16] describes grain size in diffraction as $L = k\lambda/\Delta(2\theta)_{\text{size}} \cos\theta$, where k is the Scherrer constant and $\Delta(2\theta)_{\text{size}}$ the fwhm in (2θ) at a constant wavelength λ, in angular dispersive mode. By differentiating Bragg's diffraction equation, $\lambda = 2d \sin\theta$, with respect to d and 2θ, respectively, it becomes $\Delta(2\theta) = -2(\Delta d/d) \tan\theta$. We thus rewrite the Scherrer formula in d-spacing, $L = kd^2/\Delta d_{\text{size}}$, independent of detecting mode. We substitute $\Delta d_{\text{size}} = kd^2/L$ into the Gaussian expression for the deconvoluted peak width and normalize the formula to a general definition of overall strain $\Delta d/d$, thus

$$\Delta d_{\text{obs}}{}^2/d^2 = (\epsilon^2 + \Delta d_{\text{ins}}{}^2/d^2) + (\kappa/L)^2\, d^2(P,T) \qquad (2)$$

The ordinate intercept of the $\Delta d_{\text{obs}}^2/d^2$ versus d^2 (P,T) plot for a number of *hkl* diffraction indexes presents the apparent strain, $\epsilon_{\text{apparent}}^2 = (\epsilon^2 + \Delta d_{\text{ins}}^2/d^2)$, which includes the applied strain as well as the instrument contribution (that is, the intrinsic peak-width due to instrument characteristics). This approach is a further derivation of the Williamson−Hall (WH) plot for microstrain analysis using angular dispersion 2θ mode.[17] It normalizes the WH plot with respect to d^2,

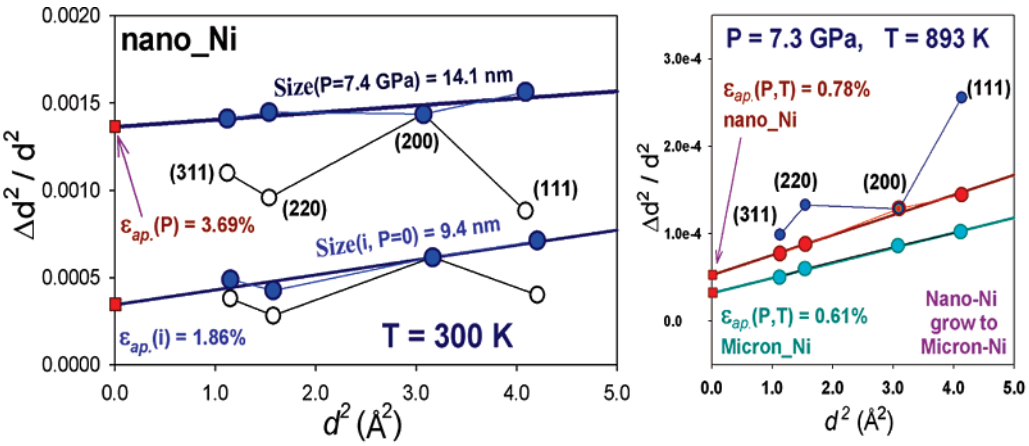

Figure 3. The plot of $\Delta d^2_{obs}/d^2$ versus d^2 (P,T) according to eq 2. Left: The highly scattered raw data of nano-Ni are shown as the open black circles and the data corrected by $DER^2 = (E_{hkl}/E_{200})^2$ are shown as solid blue symbols. The linear regression results of the DER^2 corrected data at $P = 0$ and $P = 7.4$ GPa are shown by the straight lines, whereas the ordinate receipts provide apparent strains and the plot slopes provide gain size information. Right: The raw data at high $P-T$ conditions of 7.3 GPa and 893 K for nano-Ni and micron-Ni are plotted as the red and cyan solid symbols, respectively. It is clear that all the raw data line up quite nicely at this high-T and no DER^2 corrections are needed (*DER^2 corrected data in blue are shown for reference purposes*). Notice the significant scale differences between the left and right panels; the data in the right plot would be virtually flat at the bottom in the left plot. The much smaller values of the intercept and slopes for the high $P-T$ plots indicate the great reduction of microstrain and that the nano-Ni grains grow into the micron region.

and the uncertainties associated with instrument calibrations, residual stresses, and the initial grain sizes are practically minimized. The grain size, L, is inversely proportional to peak width and can be derived from the slope $(k/L)^2$ of the $\Delta d^2_{obs}/d^2$ versus d^2 (P,T) plot. Gerward et al. have applied a similar approach to obtain grain size in energy dispersive mode,[14] where they plot β_s/E versus d-spacing in their Figure 3. In earlier studies we demonstrated that the peak-width approach works well to derive high-P induced microstrain and particle size reduction (*grain crushing under loading*) for hard and brittle ceramics and minerals (see our high $P-T$ synchrotron X-ray diffraction studies[18,19]).

Plotted in Figure 3 are normalized peak-width $\Delta d^2_{obs}/d^2$ against d^2 (P,T) for three typical data sets of ambient P ($P = 0$) and high P ($P = 7.4$ GPa), and high $P-T$ ($P = 7.3$ GPa, $T = 893$ K). Noticeably, the observed raw data (open black circles) for the nano-Ni scatter significantly as shown in Figure 3(left) and these scatterings are augmented as pressure increases. Such large data scatter is not observed in the micron-Ni sample or other micron-scale-based experiments on ceramics and minerals.[17−19] Increasing pressure also leads to increased scatter in the micron-Ni data; however, not to the level of the nano-Ni. We observe apparent variation in lattice strains according to different (hkl) diffraction planes and one cannot draw a simple straight line through the data to derive the microstrain and grain size from the plot. The fact that the (111) planes are not strained as much as the (200) planes reflects the lower elastic compliance of the (111) when comparing the details of the lattice deformation.

Hooke's law relates the stress and strain tensors by $\epsilon_{ij} = s_{ijmn}\sigma_{mn}$, where s is the elastic compliance. The stress components in our high-pressure experiments are close to quasi-isotropic, $\epsilon = [(1 - 2\nu)/E]\sigma$, where ν is the Poisson's ratio and E is Young's modulus. The diffraction elastic compliances S_1 and S_2 of the individual (hkl) planes for the nickel metal are derived using single-crystal elastic constants for nickel[20] and the mean field approach of Gnäupel−Herold et al.[21] We further derive Young's modulus $E_{hkl} = 1/(S_1 + {}^1/_2S_2)$ for different lattice planes based on the elastic compliance data, and then normalize them to an E_{hkl}/E_{200} ratio obtaining: $E_{111}/E_{200} = 1.331$, $E_{200}/E_{200} = 1.000$, $E_{220}/E_{200} = 1.229$, $E_{311}/E_{200} = 1.132$, respectively. By multiplying the square of the diffraction elasticity ratio, $DER^2 = (E_{hkl}/E_{200})^2$, to the observed raw data, we correct the strain differences on individual lattice planes. By choosing the most compliant planes as our reference, the (200) peaks, we effectively obtain the upper bound for the apparent strain. The corrected data (solid blue circles) can be readily fit to a straight line in the $\Delta d^2_{obs}/d^2$ versus d^2 (P,T) plot and allow us to derive the apparent strain and grain size information unambiguously (Figure 3). At ambient-P conditions, the initially derived apparent strain is 1.86% for the nano-Ni and 0.71% for the micron-Ni. At $P = 7.4$ GPa, the apparent strain for the nano-Ni almost doubles to 3.69% due to the applied stress. The corresponding high-P strain for the micron-Ni has a ~50% increase. At $T = 893$ K, the apparent strain is 0.78% for the nano-Ni and 0.61% for the micron-Ni, both are significantly lower than the initial states, and the nanograin grows to micrometer sizes.

By applying the DER^2 correction, we effectively eliminate/minimize the possible effects of changes in diffraction elasticity associated with the nanoscale and the pressure/temperature effects on the individual elastic moduli. The large scatter in the observed strains is due to the different hkl elastic compliances of the crystal lattice and it also reflects high surface energy of the nanoscale particles. The correction using the ratio of diffraction elastic constants is applicable to the nano-Ni but not the micron-Ni, as the contact-stress level is much higher in the nano-Ni. The magnitude of elastic correction may be a good indication of the corresponding surface strain of the nanocrystalline grains. Plotted in Figure 3(right) is a selected data set observed at

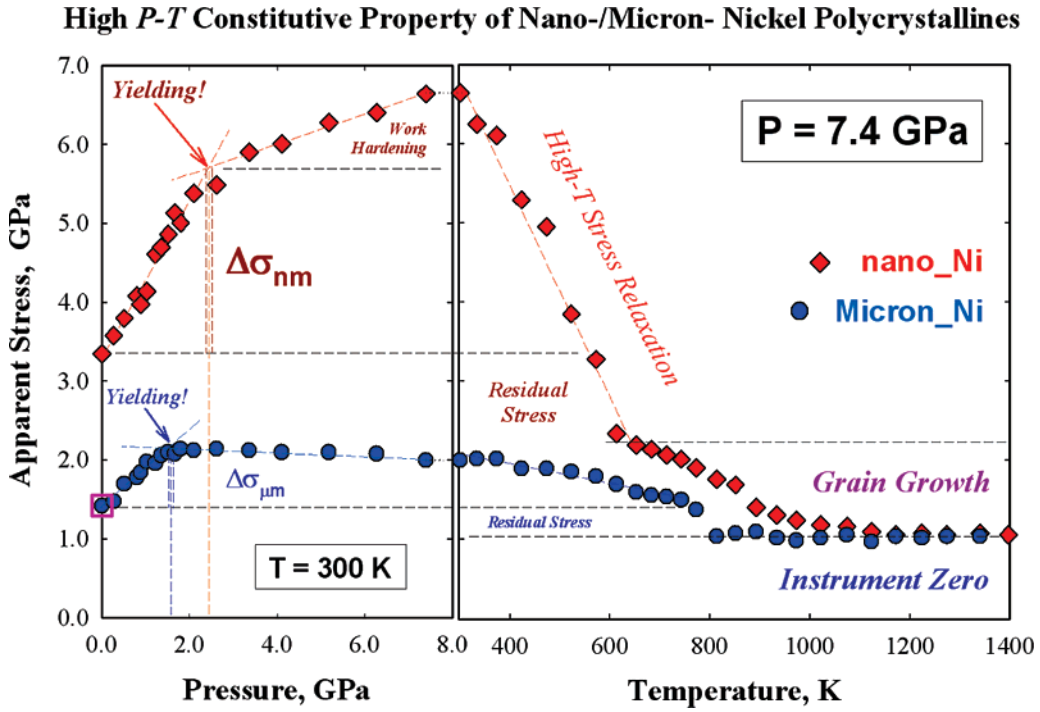

Figure 4. Apparent stresses for nano-Ni and micron-Ni plot as functions of pressure (left panel) and temperature (right panel), which include both microstrain and instrument-zero effects. The "yielding" points are derived by the intersections of elastic loading and plastic work-hardening/softening stages. The onset pressures for the yielding are apparently different for the two samples. The corresponding high-P yield-strengths are the stress differences $\Delta\sigma$ between the yielding and the initial states. The labels of *high-T stress relaxation* and *grain growth* are indicated to distinguish the dominant mechanisms at different temperature stages. The residual stresses of the samples should be extracted from the instrument-zero to the initial stress states at the ambient conditions. The purple open-square symbol is to mark the recovered samples, which return completely to the initial micron-Ni in terms of stress/strain and grain sizes. Pressure has a noticeable decrease of 0.1−0.2 GPa at high temperatures due to the cell assembly adjustments; however, the derived stress relaxations for the grain-to-grain contacts are much more significant, about 10-fold bigger for the micron-Ni and over 50-fold for the nano-Ni. The plot shows a strong comparison of constitutive properties of nano-Ni and micron-Ni under high $P-T$ conditions.

$T = 893$ K and $P = 7.3$ GPa. It is clear that all the raw data correlate linearly at high temperature as the stress level again becomes very low and the grain size coarsens into the micron regime at this high temperature.

Apparent strains have been derived for nano-Ni/micron-Ni samples and for all high-pressures/high-temperatures observed. The strains are then converted to stresses via $\sigma = E\epsilon$, and the Young's modulus applied in the conversion is $E = 180$ GPa for the nano-data and $E = 200$ GPa for the micron-data. This is because of an observed 10% reduction in the elastic modulus derivation from our recent EOS (equation-of-state) study of nano-Ni.[22] However, the pressure and temperature derivatives on the elastic modulus are still ignored, which should not affect the observation for the overall trend. The apparent stresses are plotted as a function of pressure and temperature in Figure 4 to show thermomechanics comparisons between nano-Ni and micron-Ni. The initial difference between nano-Ni and micron-Ni is thought to be due to residual stress, surface strain, and grain size effects. As pressure increases, the grain-to-grain contact stresses enhance at a much greater rate in the nano-Ni during the elastic−plastic transition region—in the stage from "micro/local" to "macro/bulk" yielding.

As the entire sample starts to lose its strength to support differential/shear stress, it is subjected to macro/bulk yield, and plastic deformation and/or viscous flow begins. Correspondingly, the diffraction peak widths do not vary as much after the bulk of the sample yields, indicating that the dislocation density in the crystalline sample reaches certain saturation. The derived yield strength of high-P *triaxial compression* is $\Delta\sigma_{\text{yield}}^{\text{nm}} \approx 2.35$ GPa for the nano-Ni, which is about the same as the uniaxial tensile strength of 2.25 GPa determined by Budrovic et al.[15] The corresponding bulk yield strength (*compression*) of micron-Ni is $\Delta\sigma_{\text{yield}}^{\mu\text{m}} \approx 0.75$ GPa, about a factor of 3 smaller than that of the nano-Ni. These observations are consistent with the classic Hall−Petch law,[7,8] which indicates a significant increase in the strength of the polycrystals as grain size decreases to the nanometer scale. The onset pressure for bulk yielding in micron-Ni at $P_{\text{yield}}^{\mu\text{m}} \approx 1.6$ GPa is also smaller than that for the nano-Ni at $P_{\text{yield}}^{\text{nm}} \approx 2.4$ GPa (Figure-4(left)). In the plastic stage, continuous peak broadening indicates strain hardening, whereas peak sharpening indicates strain softening, dynamic recovery, and/or inhomogenous plastic deformation, such as shear bonding, under certain high $P-T$ conditions. There is an evident work hardening for the nano-Ni, where the sample is seen to sustain higher differential/shear stresses after the yielding, and another $\Delta\sigma_{\text{nm}} \approx +1.0$ GPa is further loaded as the pressure increases to $P = 7.4$ GPa. However, the micron-Ni sample experiences a minor work softening at the high pressures. It is well-known that nano-metals display significantly reduced levels of work hardening than micron-scaled

metals subjected to uniaxial tensile loading. Budrovic et al.[15] observed very limited strain hardening in nano-Ni due to suppressed accumulation of dislocations after the plastic yielding. Our triaxial compression data show opposite phenomenon, which may be because of pressure effects. It is unlikely from the artifacts, due to the plot of ϵ_{ap} versus P (rather than conventional σ versus ϵ), since the work hardening/softening is observed in a comparative sense for the nano/micron samples under identical $P-T$ conditions.

The stresses exerted upon the nickel metals are drastically reduced for an initial temperature increase of $\Delta T = 300$ K, the stress relaxation is as much as $\Delta\sigma_{nm} \approx -4.5$ GPa for this ΔT increment, Figure 4(right). The further stress reduction occurs at $T > 600$ K and the stress-free states is reached at about $T > 1100$ K for the nano-Ni, while it takes place at $T \geq 800$ K for the micron-Ni. The stress level for nano-Ni at $T = 600$ K and $P = 7.4$ GPa is even lower than the initial state at the ambient conditions, indicating the removal of surface strain and annealing of residual stress of about $\Delta\sigma_{res}^{nm} \approx -1.2$ GPa at this stage. We apply identical Young's modulus of $E = 180$ GPa for both samples at temperatures of $T > 800$ K, assuming a 10% reduction in micron-Ni elasticity due to the high-T effect. The gradual stress relaxation in the micron-Ni is not as severe as in the nano-Ni and the total stress removal of $\Delta\sigma_{\mu m} \approx -1.15$ GPa (applied + residual) occurs at about $T = 800$ K. The derived residual stress for micron-Ni is about $\Delta\sigma_{res}^{\mu m} \approx 0.35$ GPa; this is the stress the crystals experience at the ambient conditions. The plot still shows minor apparent strain and grain-size effects for the nano-Ni in comparison to the micron-Ni data at this high $P-T$ condition. The direct peak width comparisons clearly show that the diffraction peaks of the nano-Ni at $T > 900$ K and $P = 7.3$ GPa are already sharper than the initial micron-Ni at ambient conditions (Figure 1), indicating both stress relaxation and grain growth. It should be pointed out that both effects occur simultaneously during the temperature increase, we label the *high-T stress relaxation* and the *grain growth* at different temperature stages to indicate the corresponding dominating mechanism.

A further reduction of residual stress of about $\Delta\sigma_{res}^{nm} \approx -1.25$ GPa occurs in the range of $T = 600-1200$ K for the nano-Ni sample (Figure 4(right)). The high-temperature data in the final portion of the experiment at $T > 1200$ K show a complete merging of nano-Ni and micron-Ni in terms of stress/strain as well as grain size. The corresponding apparent strain is due to the instrument resolution $\epsilon_{ap}^2 = \Delta d_{ins}^2/d^2$, and thus there are no effects of microstrain and grain size in this stage. The recovered micron-Ni samples after the high $P-T$ cycling have a finite peak broadening identical to the initial one at the ambient conditions, indicating that the recovered high $P-T$ sintered forms have the same residual stress level as the initial loose powder of crystalline grains. It demonstrates that there are intrinsic distributions of residual stress and grain sizes for the nickel metals under the experimentally constrained $P-T$ conditions and loading/recovery kinetics. The sample after the high $P-T$ run (recovered to ambient conditions) has a recoverability of 100%, as grains grow from nano to micron size, indicating a total strain recovery to the initial state of loose micron-Ni powder. It apparently differs from the high-P/room-T runs where the recoverability ranging from ~50% (micron-Ni) to 85% (nano-Ni) (Figure 2). High-temperature effectively annealed the residual strain and eliminated the dislocation-density generated by the high-pressure loading. The 100% recoverability of the recovered micron-Ni after the high $P-T$ cycling shows intrinsic residual strains at the initial/recovered states, reflecting similar dislocation density to the loose micron-crystal grains.

The grain sizes derived from the slope of the plot of $\Delta d_{obs}^2/d^2$ versus d^2 (P,T) show that there is no apparent grain growth in the linear elastic loading stage. After the plastic yielding at $P = 2.4$ GPa, a quite intriguing grain growth of the nano-Ni at room temperature can be derived for the data points (Figure 3(left)), by as much as ~50% at the $P = 7.4$ GPa. High-pressure usually suppresses diffusion and enhances viscosity—it actually causes grain crush in hard and brittle materials—resulting in size reduction in most ceramics and minerals.[6,18,19] For the ductile nano-Ni metal, the observed grain growth in the plastic-yielding/viscous-flowing stage under compression is thought to be due to "cold-welding". As shown in the peak intensity variations, there are apparent texture developments in the sample related to preferred orientations of the crystal grains. The atomic diffusion and lattice rotation among the crystals, driven by severe deviatoric stress, consume the "unpreferred" nano-grains and result in effective grain growth. Our observations agree with those previously discussed in the Shan et al.'s study[23] that found that grain growth occurs in nano-Ni upon straining, because of nanograins rotation during plastic deformation. Temperature increase further activates the crystal's "welding" mechanism suppressed by high pressure. The rapid sharpening of the diffraction peaks not only points to the drastic stress relaxation but also reflects the coexisting grain growth.

As discussed earlier, the microstrain in coarse-grained materials is usually attributed to the presence of strong stresses at the contact points between individual grains. In nanocrystals, which are generally viewed to consist of two structurally distinct components,[1,24] a crystalline core and a surface layer with the reduced ("strained") atomic density, the microstrain may also arise from the difference in elastic properties between these two components.[24] As crystallites gradually grow with increasing temperature, the distinction between these two components is expected to diminish, as evidenced by the lattice volume converge for nano-Ni and micron-Ni at $T > 600$ K in measurements at both zero pressure and $P = 7.4$ GPa (to be published elsewhere). This may also explain the more rapid decrease of the strength with increasing temperature in nano-Ni as compared with micron-Ni (Figure 4). To take this interpretation one step further, one can infer that a significant portion of the observed strain under compression may be due to the mismatch between crystalline core and surface layer of nickel nanocrystals.

Constitutive properties of materials under high $P-T$ conditions are important parameters in quantifying material

performance under extreme conditions, such as plate tectonics and/or dynamic shocks.[10,28] Yield strength (σ_y) is an important constitutive property of materials to define the onset of plastic deformation and viscous flow. While uncommon, the yield strengths of crystalline materials as a function of simultaneous high $P-T$ have been documented previously. The in situ and real-time synchrotron X-ray diffraction study of a material's constitutive properties is essential for the better understanding of plasticity mechanisms under high pressures/temperatures. The high-P work upon the micron-Ni is dissipated as heat during loading−unloading loop. The lower energy-dissipation for the nano-Ni indicates that the nanostructured materials can endure much greater mechanical fatigue. The stress in nano-Ni decreases as defects decrease during temperature increase, while grain growth further sharpens the diffraction peak. The slope change in Figure 4 at high pressures ($P > 2.4$ GPa) and high temperatures ($T > 600$ K) indicates the transition in the dominate mechanisms from elastic loading to plastic yield and from high-T stress relaxation to ductile grain growth, respectively. Distinguishing the different stages in the nano-Ni under high $P-T$ conditions demonstrates the effectiveness of utilizing the $\Delta d^2_{obs}/d^2$ versus d^2 (P,T) plot and the DER[2] corrections using the diffraction elastic constants for the *hkl* reflections. To be thorough, we also applied the Couchy formula, Williamson−Hall plot, and the Ungar approach for the peak-width analysis,[25−27] and the derived trends seem to be very similar to what are shown in Figure 4, however with relatively large differences in magnitude. The method described here provides excellent data interpretation not only for its rational magnitude scales in thermomechanics but also for its sensible evolvements of grain size at high $P-T$, hence revealing novel phenomena significant to nanoscience and nanotechnology.

Acknowledgment. This research is supported by Los Alamos National Laboratory, which is operated by Los Alamos National Security LLC under DOE Contract DE-AC52-06NA25396. The experimental work was carried out at beam line X17B2 at the National Synchrotron Light Source, Brookhaven National Laboratory, which is supported by the Consortium for Materials Properties Research in Earth Sciences (COMPRES) under NSF Cooperative Agreement EAR 01-35554.

References

(1) Gleiter, H. Nanocrystalline materials. *Prog. Mater. Sci.* **1989**, *33*, 223.
(2) Goldstein, A. N.; Echer, C. M.; Alivisatos, A. P. Melting in semiconductor nanocrystals. *Science* **1992**, *256*, 1425.
(3) Shen, T. D.; Koch, C. C.; Tsui, T. Y.; Pharr, G. M. On the elatic moduli of nanocrystalline Fe, Cu, Ni, and Cu-Ni alloys prepared by mechanical milling/alloying, *J. Mater. Res.* **1995**, *10*, 2892.
(4) Chen, C. C.; Herhold, A. B.; Johnson, C. S.; Alivisatos, A. P. Size dependence of structural metastability in semiconductor nanocrystals. *Science* **1997**, *276*, 398.
(5) Van Buuren, T.; Dinh, L. N.; Chase, L. L.; Siekhaus, W. J.; Terminello, L. J. Changes in the electronic properties of Si nanocrystals as a function of particle size. *Phys. Rev. Lett.* **1998**, *80*, 3803.
(6) Jiang, Q.; Pantea P.; Zhang J.; Zhao, Y.; Wang, Y.; Uchida, T. Strength of α-Si_3N_4. *J. Am. Ceram. Soc.* **2005**, *88*, 903.
(7) Hall, E. O. The deformation and ageing of mild steel III. Discussion of results. *Proc. Phys. Soc. London, Ser. B* **1951**, *64*, 747.
(8) Petch, N. J. Cleavage strength of polycrystals. *J. Iron Steel Inst.* **1953**, *174*, 25.
(9) Minor, A. M.; et al. A new view of the onset of the plasticity during the nanoidentation of aluminum. *Nat. Mater.* **2006**, *5*, 697.
(10) Weidner, D. J.; et al. Characterization of stress, pressure and temperature in SAM85, a DIA type high pressure apparatus. In *High-Pressure Research: Application to Earth and Planetary Sciences*; Syono, Y., Manghnani, M.H., Eds.; Geophysics Monograph Series; AGU: Washington DC, 1992; Vol. 67, pp 13−17.
(11) Decker, D. L. High-pressure equation of state for NaCl, KCl and CsCl. *J. Appl. Phys.* **1971**, *42*, 3239−3244.
(12) Westwood, A. D.; Murray, C. E.; Noyan, I. C. In-situ study of dynamic structural rearrangements during stress relaxation. *Adv. X-Ray Anal.* **1995**, *38*, 243.
(13) Weidner, D. J. Rheological studies at high pressure. In *Ultrahigh-Pressure Mineralogy: Physics and Chemistry of the Earth's Deep Interior*; Hemley R. J., Mao H. K., Eds.; Mineralogical Society of America: Washington, DC, 1998; pp 493−524.
(14) Gerward, L.; Morup, S.; Topsoe, H. Particle size and strain broadening in energy-dispersive x-ray powder patterns. *J. Appl. Phys.* **1976**, *47*, 822.
(15) Budrovic, Z.; Van Swygenhoven, H.; Derlet, P. M.; Van Petegem, S.; Schmitt, B. Plastic deformation with reversible peak broadening in nanocrystalline nickel. *Science* **2004**, *304*, 273
(16) Patterson, A. L. The Scherrer Formula for X-Ray Particle Size Determination. *Phys. Rev.* **1939**, 56, 978.
(17) Williamson, G. K.; Hall, W. H. X-ray line broadening from filed aluminum and wolfram. *Acta Metall.* **1953**, *1*, 22.
(18) Zhang, J.; Wang, L.; Weidner, D. J.; Uchida, T.; Xu, J. Strength of moissanite. *Am. Mineral.* **2002**, *87*, 1005−1008.
(19) Chen, J.; Schmidt, N.; Chen, J. H.; Zhang, J.; Wang, L.; Weidner, D. J. Yield Strength Enhancement of MgO by Nanocrystals. *J. Mater. Sci.* **2005**, *40*, 5763.
(20) Simmons, G.; Wang, H. *Single Crystal Elastic Constants*; MIT Press: Cambridge, MA, 1971.
(21) Gnäupel-Herold, T.; Brand, P. C.; Prask, H. J. Calculation of single-crystal elastic constants for cubic crystal symmetry from powder diffraction data. *J. Appl. Crystallogr.* **1998**, *31*, 929.
(22) Zhang, J.; Zhao, Y.; Palosz, B. Comparative studies of compressibility between nanocrystalline and bulk nickel. *Appl. Phys. Lett*., in press.
(23) Shan, Z. W.; Stach, E. A.; Wiezorek, J. M. K.; Knapp, J. A.; Follstaedt, D. M.; Mao, S. X. Grain boundary-mediated plasticity in nanocrystalline nickel. *Science* **2004**, *305*, 654.
(24) Palosz, B. High-pressure x-ray diffraction studies on nanocrystalline materials. *J. Phys. Condens. Mater.* **2003**, *15*, 1.
(25) Ungar, T.; Tichy, G. Effect of dislocation contrast on X-ray line profiles in untextured polycrystals. *Phys. Status Solidi A* **1999**, *171*, 425.
(26) Ungar, T.; Dragomir, I.; Revesz, A.; Borbely, A. The contrast factors of dislocations in cubic crystals: the dislocation model of strain anisotropy in practice. *J. Appl. Crystallogr.* **1999**, *32*, 992.
(27) Shen, T. D.; Schwarz, R. B.; Thompson, J. D. Soft magnetism in mechanically alloyed nanocrystalline materials. *Phys. Rev. B* **2005**, *72*, 014431.
(28) Feng, R.; Raiser, G. F.; and Gupta, Y. M. Material strength and inelastic deformation of silicon carbide under shock wave compression. *J. Appl. Phys.* **1998**, *83*, 79.

NL062685S